Electro, Physical & Theoretical Chemistry

Comparative MD Study of Inhibitory Activity of Opaganib and Adamantane-Isothiourea Derivatives toward COVID-19 Main Protease M^{pro}

Jelena Đorović Jovanović,*[a] Marko Antonijević,[a] Ali A. El-Emam,[b] and Zoran Marković[a]

In this study, the inhibitory potency of four adamantly-isothiourea derivatives (compounds **1** [4-bromobenzyl (Z)-N′-(adamantan-1-yl)-4-phenylpiperazine-1-carbothioimidate], **2** [3,5-bis(trifluoromethyl)benzyl (Z)-N′-(adamantan-1-yl)-4-phenylpiperazine-1-carbothioimidate], **3** [4-bromobenzyl (Z)-N-(adamantan-1-yl)morpholine-4-carbothioimidate] and **4** [3,5-bis (trifluoromethyl)benzyl (Z)-N-(adamantan-1-yl)morpholine-4-carbothioimidate]) was evaluated against SARS-CoV-2 targeted proteins. The investigated compounds **1**–**4** possess a similar structure to opaganib, which is used in studies like a potential drug for COVID-19 treatment. Since examined adamantly-isothiourea derivatives (**1**–**4**) shown broad-spectrum of antibacterial activity and significant *in vitro* cytotoxic effects against five human tumor cell lines and shown similarity in structure with opaganib, it was of interest to study their inhibitory potency toward some SARS-CoV-2 proteins such as SARS-CoV-2 main protease M^{pro} and mutation of SARS-CoV-2 Spike (S) Protein D614G. The inhibitory potency of studied compounds is examined using molecular docking and molecular dynamic simulations. The results of molecular docking simulations indicate compound **1** as the most prominent candidate of inhibition of SARS-CoV-2 main protease M^{pro} ($\triangle G_{bind} =$ 11.24 kcal/mol), while almost the same inhibition potency of all studied compounds is exhibited toward D614G. Regarding the results obtained by molecular dynamic simulations, compounds **1** and **4** possess similar inhibitory potency toward SARS-CoV-2 main protease M^{pro} as opaganib ($\triangle G_{bind} \approx$40 kcal/mol).

Introduction

At the end of the year 2019, the novel coronavirus infection, named SARS-CoV-2, is detected in Wuhan, China. The World Health Organization (WHO) has announced a global emergency and pandemic of COVID-19 diseases caused by SARS-CoV-2 virus. Human Coronaviruses (HCoVs) are already known family of viruses and they are recognized as pathogens that can be the source of a wide range of diseases, and they found the ability to easily mutate and infect other species.[1,2] Until the emergence of COVID-19, six human coronaviruses belonging to Alphacoronaviruses (HCoV-NL63 and HCoV-229E) and Betacoronaviruses (HCoV-OC43, HCoV-HKU1, SARS-CoV, MERS-CoV) are defined.[3] The newly detected coronavirus disease (COVID-19) is an infectious disease caused by the coronavirus from a group of Betacoronaviruses, SARS-CoV-2.

On May 17, 2021, according to the World Health Organization, this virus is confirmed in 220 countries, 162,773,940 infected cases are detected, 3,375,573 are with fatal consequences and about 140,000,000 people are recovered. The patients that suffer from COVID-19 have a different clinical picture, from mild symptoms to severe illness, and symptoms may appear 2–14 days after exposure to the virus. The characteristic symptoms are fever, cough, shortness of breath, muscle pain, headache, sore throat, and loss of taste or smell. At a venture, a huge group of infected individuals have mild upper respiratory tract problems and recover without special treatment. Patients with pre-existing health problems have more severe respiratory problems.[4] The huge problem in this epidemic is missing specific treatment for the new virus.[5,6] The whole academic community is working intending to elucidate the new virus and the pathophysiology of the disease and to discover effective therapeutic agents and vaccines.[7–14] Also, this emergency made scientists develop different models for the predictions on the influence of COVID-19 on the world population.[15,16]

While traditional methods of drug discovery may take a few years, the *in silico* models help in the prediction of possible inhibitors in a short time. Treatment of COVID-19 can follow the blocking binding of the virus to human cell receptors or inhibiting the virus's self-assembly process through acting on some structural proteins to prevent the synthesis of viral RNA through acting on the genetic material of the virus, inhibiting virus replication through acting on critical enzymes of the virus.

Opaganib (ABC294640, **OPG**), an adamantane-based anticancer drug that acts as an inhibitor of the enzyme Sphingosine-2-kinase (SK).[17–22] SK is recognized as a receptor that allows activation and regulation of mast cells which mediates sphingosine-1-phosphate production, thus allowing calcium influx, cytokine production, NF-κB activation.[23] OPG is

[a] *Dr. J. Đ. Jovanović, M. Antonijević, Z. Marković*
Department of Science, Institute for Information Technologies, University of Kragujevac, Jovana Cvijića bb, 34000 Kragujevac, Republic of Serbia
E-mail: jelena.djorovic@uni.kg.ac.rs
[b] *Prof. A. A. El-Emam*
Department of Medicinal Chemistry, Faculty of Pharmacy, Mansoura University, Mansoura 35516, Egypt

Supporting information for this article is available on the WWW under https://doi.org/10.1002/slct.202101898

under development as a potential treatment agent for several different kinds of cancer.[17–22] In addition, **OPG** is a selective inhibitor with anti-inflammatory and antiviral properties.[24,25] The anti-inflammatory and antiviral properties of **OPG**, together with a good safety profile, have driven the use of OPG under an expanded access program on seven Israeli COVID-19 patients with severe disease. It is reported treatment and comparison on the patients' reaction to those of untreated COVID-19 patients with similar disease severity.[26] Recently, the FDA has approved the application for a phase 2, randomized, double-blind, and placebo-controlled study to evaluate **OPG** effect at patients with moderate-to-severe SARS-CoV-2 pneumonia [NCT04414618].[26] There are findings that inhibitors such as OPG, Ifenprodil, CM4620-IE, and numerous other treat cytokine storm.[27]

In a previous study, a series of adamantane-linked isothiourea derivatives were synthesized,[28] which have been found to exhibit potent broad-spectrum antibacterial activity. Since these newly-synthetized compounds are structurally related to OPG, it was of interest to study its inhibitory potency toward some SARS-CoV-2 responsible proteins. Like OPG, these derivatives were recently reported to possess marked *in vitro* and *in vivo* anticancer activity.[29] The examined adamantyl isothiourea derivatives shown *in vitro* cytotoxic effects against five human tumor cell lines.[29]

In this study, the physicochemical and pharmacokinetic properties of the studied compounds are considered. Further, the binding potential between **OPG** and the synthesized compounds **1** [4-bromobenzyl (Z)-N′-(adamantan-1-yl)-4-phenylpiperazine-1-carbothioimidate], **2** [3,5-bis(trifluoromethyl) benzyl (Z)-N′-(adamantan-1-yl)-4-phenylpiperazine-1-carbothioimidate], **3** [4-bromobenzyl (Z)-N-(adamantan-1-yl) morpholine-4-carbothioimidate] and **4** [3,5-bis(trifluoromethyl) benzyl (Z)-N-(adamantan-1-yl)morpholine-4-carbothioimidate] (Figure 1) towards SK, SARS-CoV-2 main protease M^{pro} and mutation of SARS-CoV-2 Spike (S) Protein D614G, is determined using molecular docking simulations regarding potential interactions between this compounds and targeted proteins. To evaluate the interactions between the ligands (**OPG**, **1**, **2**, **3**, and **4**) with the SARS-CoV-2 major protease M^{pro}, molecular dynamics (MD) simulation was used.

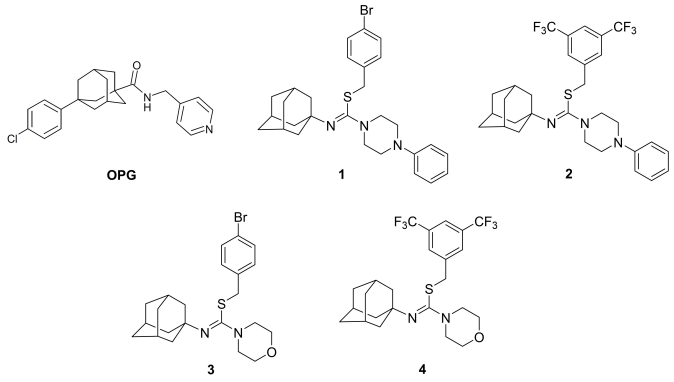

Figure 1. Structures of investigated compounds used as ligands in molecular docking and dynamic simulations.

Main protease M^{pro} from SARS-CoV-2 is one of the key enzymes of coronaviruses and has a pivotal role in mediating viral replication and transcription, making it an attractive drug target for SARS-CoV-2.[30,31] Considering this fact, there is a focus on identifying a drug that as a target protein has the main protease (M^{pro}) of SARS-CoV-2.[32] On the other hand, some findings indicate Spike (S) protein as a key protein used by the SARS-CoV-2 virus to attack the human cells.[4,33] It has also been found that the Spike (S) protein has different forms in different coronaviruses.[34] Further, some studies show that SARS-CoV-2 modification carrying the Spike protein amino acid change D614G has become the most prevalent form in the global pandemic.[35–38] The tracking of modified frequencies indicates the constant pattern of increasing G614 at multiple different levels, such as national, regional, and municipal. The changes are observed even in the local epidemic condition where the G614 variant contributes to a shift in the original D614 form. It was found that the G614 variant grows to a higher titer as pseudotyped virions, and that infected individuals have problems with higher upper respiratory tract, but this does not increase disease severity.[35] Also, every day scientists detect other proteins considered as responsible for virus impact on human health. Various studies have provided new insights, changed direction, and set new and different actions that have led to the discovery of new potential drugs for the treatment of COVID-19.[39–42]

Results and Discussion

Druglikeness analysis

The prediction of the drug-likeness is realized using The SwissADME web tool. The physiochemical properties and computation of the Absorption, Distribution, Metabolism and Excretion (ADME) parameters are performed for **OPG**, **1**, **2**, **3**, and **4**. The obtained results are presented in Table S1. The five parameters analyzed for the interpretation of Lipinski's rule are MW (molecular weight), log P (predictable permeability of the skin), HB donor (estimated number of hydrogen bonds that would be donated by the solute to water molecules in an aqueous solution), HB acceptor (estimated number of hydrogen bonds that would be accepted by solute molecules of water in aqueous solution). Drugs in some cases do not meet these rules, for example orally active therapeutic classes such as antibiotics, antifungals, vitamins, and cardiac glycosides.[43] It is known that Lipinski's rules are an important screening method for testing new compounds that can be used in treatment. According to these rules, based on the obtained results presented in Table S1, it can be concluded that the examined compounds deserve the attention of the researcher and should be subjected to further tests in order to use them for the treatment of SARS-CoV-2.

Inhibitory potency of OPG and examined adamantyl isothiourea derivatives

Molecular docking simulations

The emergence of the pandemic of COVID-19 put in the foreground research of potential drugs for the treatment of SARS-CoV-2. Some studies show that some anticancer drugs, such as **OPG**, effects the treatment of COVID-19.[26] In this paper is reported an examination of the inhibitory potency of **OPG**, **1**, **2**, **3** and **4** against COVID-19 main protease M^{pro} by the means of molecular docking and molecular dynamic analysis. The structures of studied compounds, optimized at the B3LYP-D3BJ/6-311++G(d, p) are given in Table S1. Firstly, the pockets and binding sites of targeted proteins are defined. The AGFR software was employed to compute affinity maps for a receptor molecule to be used for molecular docking simulations. In the case of M^{pro} the inhibitor N3 was removed and was accomplished binding site is determined. The obtained results of the binding pocket analysis revealed that His41, Cys145, Glu143, His163, His164 are amino acids responsible for binding. This is in agreement with experimental data.[44] Further, molecular docking simulations were performed with the **OPG**, **1**, **2**, **3**, and **4** and the same docking pose is generated as found for the N3 inhibitor. The molecular docking simulations are also performed for mutation of Spike protein D614G. For molecular docking simulations as ligands are used molecules of **OPG**, **1**, **2**, **3**, and **4**. The molecular docking simulations were also performed between **OPG**, **1**, **2**, **3**, **4** as ligands, and SK is used as protein in simulations. Since OPG is recognized as an inhibitor of the enzyme SK, it was used as a reference compound. The value of free energy of binding ($\triangle G_{bind}$) depends on the Final Intermolecular Energy (FIE), Final Total Internal Energy (FTIE), Torsional Free Energy (TFE), and Unbound System's Energy (USE) (eq. 1). The FIE is a summary of the Van der Waals energy, energy of hydrogen bonds, desolvation energy of the system, and electrostatic energy.

$$\Delta G_{bind} = [(FIE) + (FTIE) + (TFE)\text{-}(USE)] \quad (1)$$

As a matter of the value of K_i, the smaller values of the K_i indicate the greater binding affinity, and the smaller amount of drug is needed to inhibit the activity of the receptor. From the presented results, it is clear that values of $\triangle G_{bind}$ and K_i are in connection; the lower values of $\triangle G_{bind}$ are followed by lower values of K_i. The binding affinity is predicted based on the values of binding energy and inhibition constant (Tables 1, S2, and S3). The inhibitory potency of OPG, as well inhibitory potency of **1**, **2**, **3**, and **4**, is firstly investigated on the SK2 (Table S2). According to the results presented in Table S2, despite the already recognized inhibitor of SK2 is **OPG**, the most probable and with the highest inhibitory potency is **3**, since it shows the lowest values of $\triangle G_{bind}$ and K_i than. The compounds **1**, **2**, and **4** show almost the same inhibitory potency against SK2. It should be noted that interaction realized in molecular docking simulation with SK does not include hydrogen bonds (Figure S1), leading to the indication that hydrophobic contacts are responsible for inhibitory potency of examined compounds through SK. Considering this fact, it is justified to expect that results of molecular docking simulation with SARS-CoV-2 M^{pro} and D614G give the same picture. However, investigated compounds display a little bit different affinities against SARS-CoV-2 proteins.

The binding modes of investigated ligands towards SARS-CoV-2 M^{pro} and D614G are given in Tables 1 and S3. From the values of $\triangle G_{bind}$ and K_i presented in Table 1, it can be concluded that compound **1** should be the best inhibitor of M^{pro}, and the second-best inhibitor will probably be compound **3**. The highest values of binding energy and inhibition constant are obtained for compound **4**, indicating this compound as the least likely candidate for inhibition of SARS-CoV-2 M^{pro}, while compounds **2** and **3** displayed almost the same inhibition potency. **OPG**, which is the already tested drug, shows similar almost the same inhibitory potency as candidates **2** and **3**. The differences between the calculated values of $\triangle G_{bind}$ and K_i are very small, almost negligible, and only the values for compound **1** are significantly lower, which makes this compound marked as potentially the best candidate for inhibition. In support of this claim, the lower values of binding energies are obtained for here studied compounds for inhibition of SARS-CoV-2 M^{pro}, than with chloroquine.[45]

The difference in binding affinity between different ligands and proteins can be explained by the number and type of interaction. In molecular docking simulations with SARS-CoV-2 M^{pro} are notable that hydrogen bonds are achieved. The most prominent interactions are hydrogen bonds, π-alkyl and alkyl (between adamantyl ring of compounds **1**–**4** and amino acid from SARS-CoV-2 M^{pro}) (Figure 2). There are two types of hydrogen bonds that are established: conventional hydrogen bonds and carbon-hydrogen bonds. These interactions are novelty comparing the interactions of the same compounds with SK. The number of hydrogen bonds has an important role in the complete stability of complexes,[46] and some of the promising antivirals have over three hydrogen bonds formed.[47] The determined hydrogen bonds during molecular docking

Table 1. The important thermodynamical parameters from molecular docking simulations with SARS-CoV-2 M^{pro} (PDB ID: 6lu7).

	$\triangle G_{bind}$ (kcal/mol)	K_i (uM)	FIE (kcal/mol)	vdW + Hbond + desolv Energy (kcal/mol)	Electrostatic Energy (kcal/mol)	FTIE (kcal/mol)	TFE (kcal/mol)	USE (kcal/mol)
OPG	−9.54	0.10139	−10.73	−10.69	−0.04	−1.03	+1.19	−1.03
1	−11.24	0.00581	−13.03	−13.00	−0.03	−1.52	+1.79	−1.52
2	−9.95	0.05077	−12.34	−12.30	−0.04	−2.18	+2.39	−2.18
3	−10.16	0.03579	−11.65	−11.52	−0.13	−1.28	+1.49	−1.28
4	−9.37	0.13462	−11.46	−11.47	+0.00	−1.37	+2.09	−1.37

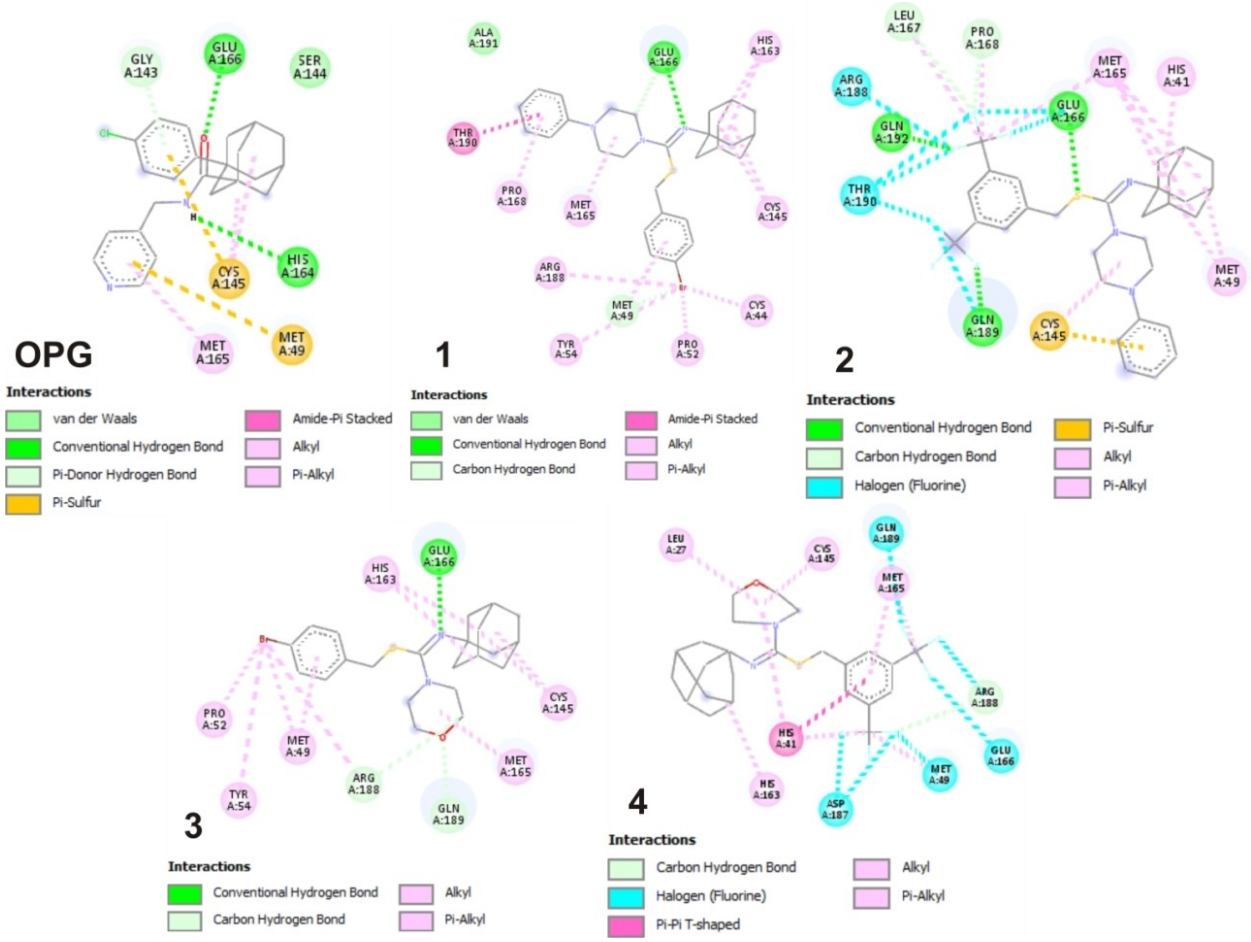

Figure 2. Interaction of investigated compounds, **OPG** and compounds **1**–**4** and with SARS-CoV-2 M^{pro}.

simulations deserve detailed analysis, and for that purpose, all protein-ligands complexes undergo molecular dynamic simulations.

The results represented in Table S3 and Figure 3 refer to interactions accomplished in molecular docking simulations of studied compounds and mutation of Spike (S) protein D614G. The values of the binding energies calculated for **1**, **2**, **3**, and **4** presented in Table S3 indicate almost the same inhibition potency toward D614G. On the other hand, OPG show significantly lower free energy of binding than corresponding examined compounds. In previously analysed molecular docking simulations this was not the case (Tables 1 and S2). This observation indicates studied compounds as potential inhibitors of D614G mutation. The obtained results of similar values of the binding energies as in the case of SARS-CoV-2 M^{pro} suggest that the mutation D614G has a significant role in COVID-19 epidemiology and the design of therapeutic treatment.

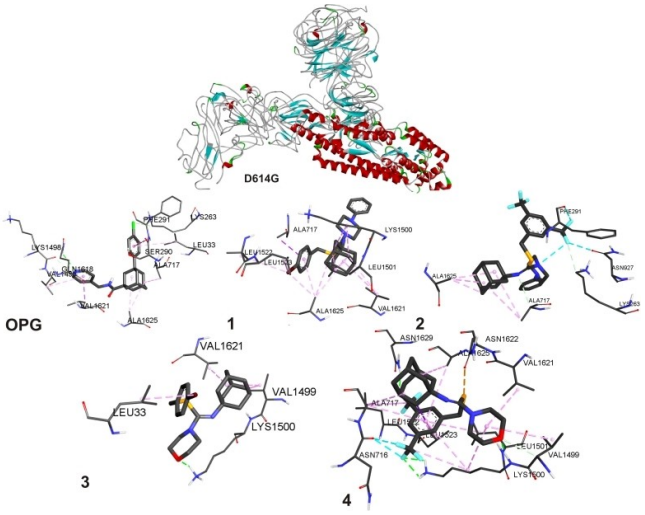

Figure 3. Structure of Spike (S) protein (D614G) and its interactions with OPG and compounds **1**–**4**.

Molecular dynamic simulations and analysis

The most stable conformations of protein-ligand complexes of investigated compounds and SARS-CoV-2 M^{pro}, the ones with the lowest values of binding energies from molecular docking simulations, are used as inputs for molecular dynamic simu-

lations. For the molecular dynamic analyses and to investigate the system properties, including the overall stability, local residue, and general structure fluctuations through the simulations Root Mean Square Deviation (RMSD), Radius of gyration (Rg), and Root Mean Square Fluctuation (RMSF) are estimated from analysis of output trajectories. These parameters are used to determine the structural stability of the protein-ligand complex in time (0-50 ns).[48,49] The changes in protein structure, concerning initial coordinates, are measured by the RMSD.

Charts shown in Figure 4 represent the RMSD values of investigated protein-ligand complexes with compounds **1**, **2**, **3**. and **4**, in comparison to the SARS-CoV-2 M^{pro}-**OPG** complex and the SARS-CoV-2 M^{pro} protein itself.

As can be seen from the RMSD charts ar Figure 4, protein-ligand complex SARS-CoV-2 M^{pro}-**2** shows the best stabilization of the protein. In support of this are estimated values of binding energies (Table 2), and the number of protein-ligand interactions, as well as hydrogen bonds, realized in this complex (Table S4). The SARS-CoV-2 M^{pro}-**2** complex reaches equilibration just after 5 ns and stays stable for all remaining 45 ns. In the case of the SARS-CoV-2 M^{pro}-**1** complex, the stabilization of protein is achieved after 40 ns, and the structure remains stable for the rest of the simulation. The RMSD of the SARS-CoV-2 M^{pro}-**4** complex pretty much follows the RMSD of the SARS-CoV-2 M^{pro}- **OPG**, but based on the RMSD it seems that the SARS-CoV-2 M^{pro}-**4** complex is more stable. This is expected since the structure of compound **4** contains two trifluoromethyl groups that are involved in a lot of interactions with amino acid residues. In the end, SARS-CoV-2 M^{pro}-**3** complex shows the most fluctuation in the RMSD diagram, and the complex gets stabilized after 45 ns. Large oscillations between 32 ns and 38 ns indicate that the ligand was adapting another confirmation within the same binding site.

Table 2. The free energies of binding of protein-ligand complexes determent by free energy workflow (FEW), according to the linear interaction energy (LIE) approach (kcal/mol).

	$\triangle G_{bind}$
ΔE(SARS-CoV-2 Mpro-OPG)	−37.8
ΔE (SARS-CoV-2 Mpro-1)	−41.5
ΔE(SARS-CoV-2 Mpro-2)	−67.9
ΔE(SARS-CoV-2 Mpro-3)	−10.8
ΔE(SARS-CoV-2 Mpro-4)	−43.1

One of the significant properties of protein function is flexibility. The more flexible proteins have expanded binding pockets which considerably influences the substrate-product kinetics and affinity.[50] The RMSF values for protein-ligand SARS-CoV-2 M^{pro} complexes, concerning RMSF values for SARS-CoV-2 M^{pro}protein alone, are showing a degree of rigidity of the system. Fluctuation is significantly lower when the ligand is bonded to protein. Inspection of Figure S2 shows that the curve of the RMSF value of SARS-CoV-2 M^{pro}-**2** complex following the RMSF values of the SARS-CoV-2 M^{pro} protein, indicating that stabilization of protein by binding of compound **2** has been achieved without an unnecessary increase in rigidity of the system.

The parameter that is associated with the size and compactness of the protein is the radius of gyration (Rg). The

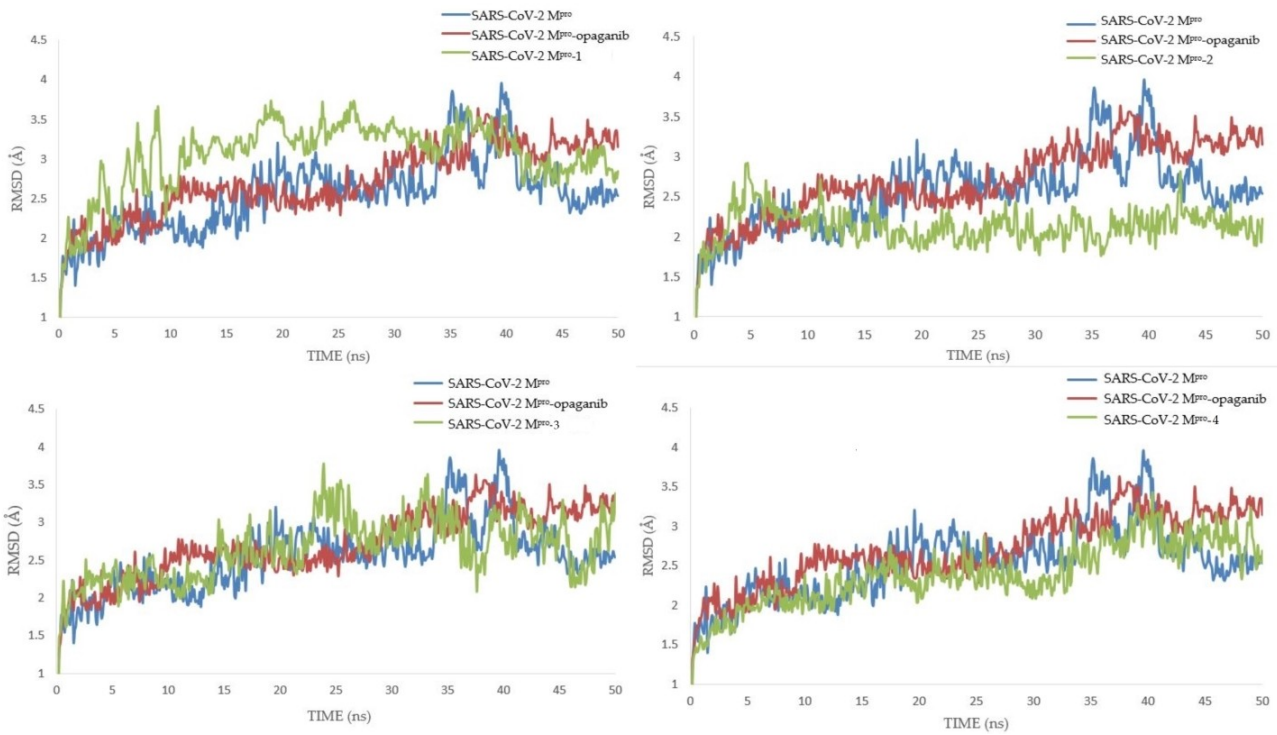

Figure 4. RMSD values of investigated complexes.

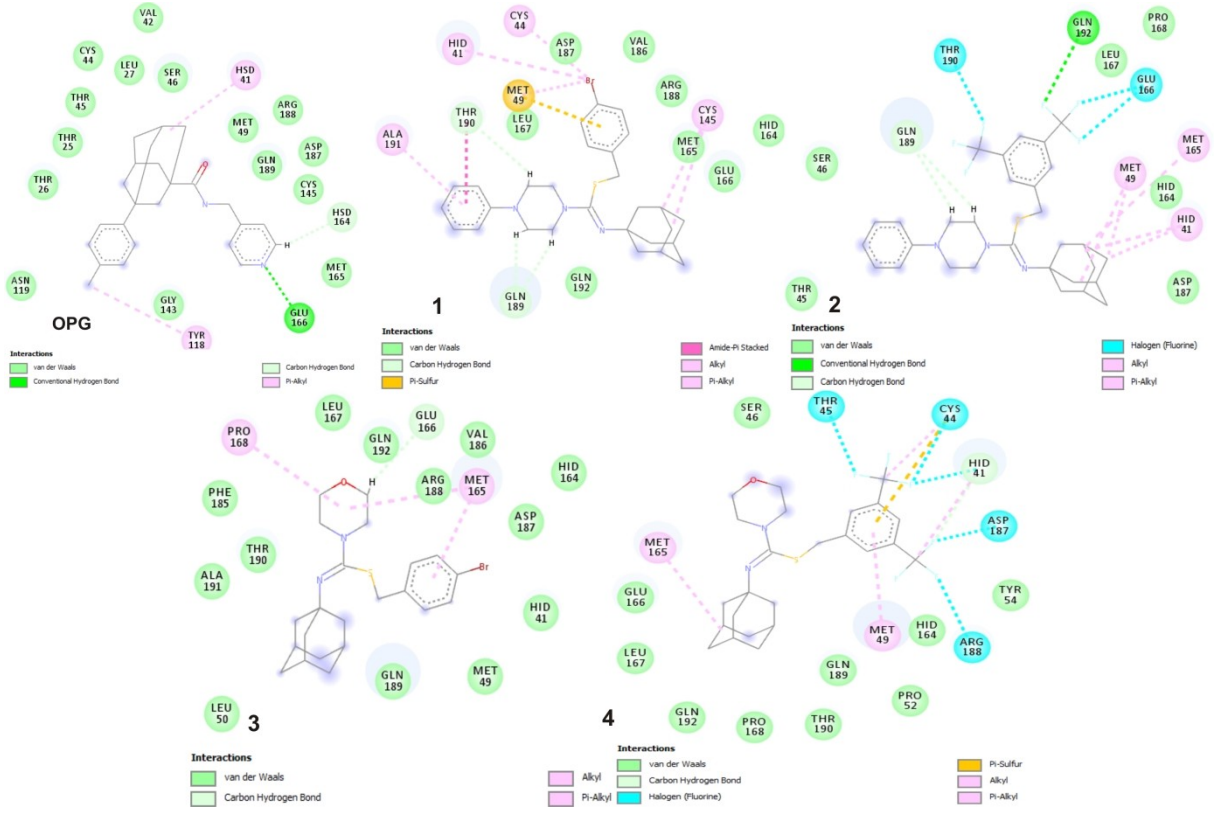

Figure 5. 2D diagrams of protein-ligand interactions after 50 ns of molecular dynamic simulations of complexes between SARS-CoV-2 Mpro and OPG, and compounds **1**–**4**.

Rg values of studied protein-ligand complexes are given in Figure S3.

As can be seen from Figure S3, Rg of SARS-CoV-2 M^{pro}-**2** complex follows the Rg of the protein, which confirms that structural changes induced by binding of compound **2** to SARS-CoV-2 M^{pro} do not cause deviations in the secondary structure of the protein. Furthermore, complexes with compounds **1** and **2** are showing similar behavior, as can be expected from their similar energies and RMSD values. Surprisingly, Rg of the complex with compound **3** does not show much deviation, which means that the low value of binding energy does not come from deviations in the secondary structure of the investigated protein.

Further analysis of molecular dynamic simulations includes the calculation of the free energies of binding (Table 2), as well as the analysis of interactions between ligands and SARS-CoV-2 M^{pro} protein (Table S4). The free energies of binding are obtained using the free energy workflow (FEW) tool which includes the linear interaction energy approach (LIE).[51,52] By this approach the binding free energy is estimated from the change in electrostatic (ele) and van der Waals (vdW) interaction energy between the ligand and the protein in the solvated model. The interaction energy contributions are determined from molecular dynamic simulations of the free protein and the protein-ligand complex. As can be seen from the results presented in Table 2, the compound with the lowest value of binding energy, among investigated compounds is compound **2**. Following, compounds **1** and **4** are showing relatively similar values of binding energies, while compound **3** has the highest value of binding energy. By examining the structures of investigated compounds, it is easy to see that presence of two CF_3 groups takes a great part in protein-ligand interactions. Compounds that contain those CF_3 groups (**2** and **4**) show lower binding energies than equivalent compounds with Br as the substituent. The values of binding energies from Table 2 suggest that the aromatic ring has a big influence on protein-ligand interactions.

As can be seen from the results presented in Table S4 regarding Table 2, the lower values of the binding energy are obtained when more interactions are involved in protein-ligand synergy. The hydrogen bonds are showing the biggest influence on protein-ligand binding energies. Another type of interaction that has a similar impact as hydrogen bonds are non-covalent interactions where length doesn't exceed 3.2 Å. The greater the length of these interactions are, the less influence they have on the value of binding energy. The protein-ligand complex SARS-CoV-2 M^{pro}-**2** builds interactions with a length around 3 Å, and this is a similar length to the length of the hydrogen bond. The strongest non-covalent interaction of compound **1** has a length of 3.8 Å. This is highly reflected in binding energies. A little bit more obvious example of the impact of non-covalent interactions on binding energies

is compound **4** in regard to compound **3**. While complexes with both compounds have one hydrogen bond, the number of non-covalent interactions, especially those with a length of 3 Å makes a lot of difference in values of binding energies. In comparison to **OPG**, compound **2** shows a significantly better affinity for binding with SARS-CoV-2 M^{pro}. Compounds **1** and **4** have quite a similar affinity for binding like **OPG**, and compound **3** has a lot lower binding potential to SARS-CoV-2 M^{pro}.

Further, if the results obtained by molecular docking simulation are analysed and compared with the results of molecular dynamic simulations, some similarities and some differences will be notice noticed. In molecular docking simulations His41, Glu143, Cys145, His163, His164 are amino acids from SARS- CoV-2 M^{pro} responsible for interactions with ligand compounds.

After 50 ns of molecular dynamic simulations, some contacts are missing while the other ones are present (Figure 2, Figure 5, and Table S4). The contacts which are stable in the time and in the presence of water molecules are established with His41, Cys145, Met165, Glu166, Gln189, and Asp187. The presence of interactions with His41 and Cys145 confirmed that SARS-CoV-2 had the Cys–His catalytic dyad (His41 and Cys145).

Conclusions

In the presented study the inhibitory potency of four adamantyl isothiourea derivatives (compounds **1**–**4**) is estimated against SARS-CoV-2 targeted proteins. According to the evaluated drug-likeness, achieved results satisficed Lipinski "rule of 5" and, imposed that investigated compounds deserve further investigation and consideration of their use for the treatment of SARS-CoV-2. Also, molecular docking simulations are performed to predict the potential inhibitory potency of compounds **1**–**4** toward SARS-CoV-2 main protease M^{pro} and mutation of SARS-CoV-2 Spike (S) Protein D614G. In addition, the inhibitory potency of examined adamantyl isothiourea derivatives is compared to the inhibitory potency of **OPG**. The results of molecular docking simulations with SARS-CoV-2 main protease M^{pro} indicate that all of the studied molecules are bound in the active position of protein, in the area of the His41-Cys145. The results from molecular docking simulations indicate compounds **1** and **3** as the potent inhibitors of SARS-CoV-2 main protease M^{pro}. The values of binding energy show that **OPG** posses better binding affinity only from compound 4. Besides, investigation of inhibitory potency of **OPG** and compounds **1**–**4**, applying molecular dynamic simulations, indicate compounds **2** and **4** as potentially best inhibitors of SARS-CoV-2 M^{pro}, since they show the lowest values of binding energy after 50 ns of simulations. As regard molecular docking simulations with Spike (S) Protein D614G, the prominent inhibitory potency shows **OPG**, while examined adamantly-isothiourea derivatives possess similar inhibitory potential between each other. This result makes the compounds **1**–**4** prominent candidates for advanced investigations for the treatment of COVID-19.

Supporting Information Summary

In Supporting Information are given Experimental Section, Table S1. Drug likeness of potential inhibitor candidates, Table S2. The important thermodinamical parameters from docking simulations with Sphingosine kinase (PDB ID: 3vzb), Figure S1. Interaction of investigated compounds with Sphingosine Kinase, Table S3. The important thermodynamical parameters from docking simulations with D614G, Table S4. The protein-ligand interactions after 50 ns of molecular dynamic simulations, Figure S2. RMSF values of investigated complexes concerning protein without ligand, and Figure S3. Rg values of investigated complexes regarding protein without ligand

Acknowledgements

The authors wish to acknowledge the Ministry of Education, Science, and Technological Development of the Republic of Serbia for the financial support through contract no. 451-03-9/2021-14/200378.

Conflict of Interest

The authors declare no conflict of interest.

Keywords: Adamantyl-isothiourea derivatives · Inhibitors · Molecular dynamics · Molecular modeling

[1] L. Van Der Hoek, K. Pyrc, M. F. Jebbink, W. Vermeulen-Oost, R. J. Berkhout, K. C. Wolthers, P. M. Wertheim-van Dillen, J. Kaandorp, J. Spaargaren, B. Berkhout, *Nat. Med.* **2004**, *10*, 368–373.
[2] C. Liu, Q. Zhou, Y. Li, L. V. Garner, S. P. Watkins, L. J. Carter, D. Albaiu, *ACS Cent. Sci.* **2020**, *6*, 315–331.
[3] A. A. Elfiky, *Life Sci.* **2020**, *248*, 117477.
[4] C. Shu, X. Huang, T. Huang, L. Chen, B. Yao, J. Zhou, C. Deng, *STEMed.* **2020**, *1*, e41-e41.
[5] O. Mitjà, B. Clotet, *LancetGH.* **2020**, *8*, e639–e640.
[6] L. Zhang, Y. Liu, *J. Med. Virol.* **2020**, *92*, 479–490.
[7] M. Hagar, H. A. Ahmed, G. Aljohani, O. A. Alhaddad, *Int. J. Mol. Sci.* **2020**, *21*, 3922.
[8] D. Gentile, V. Patamia, A. Scala, M. T. Sciortino, A. Piperno, A. Rescifina, *Mar. Drugs.* **2020**, *18*, 225.
[9] O. O. Olubiyi, M. Olagunju, M. Keutmann, J. Loschwitz, B. Strodel, *Molecules.* **2020**, *25*, 3193.
[10] J. Wang, *J. Chem. Inf. Model.* **2020**, *60*, 3277–3286.
[11] L. Zhang, D. Lin, X. Sun, U. Curth, C. Drosten, L. Sauerhering, S. Becker, K. Rox, R. Hilgenfeld, *Science.* **2020**, *368*, 409–412.
[12] R. Alexpandi, J. F. De Mesquita, S. K. Pandian, A. V. Ravi, *Front. Microbiol.* **2020**, *11*, 1796.
[13] W. R. Ferraz, R. A. Gomes, A. L. S. Novaes, G. H. Goulart Trossini, *Future Med. Chem.* **2020**, *12*, 1815–1828.
[14] X. Liu, B. Zhang, Z. Jin, H. Yang, Z. Rao, *Nature.* **2020**, *582*, 289–293.
[15] D. Štifanić, J. Musulin, A. Miočević, S. Baressi Šegota, R. Šubić, Z. Car, *Complexity.* **2020**, *2020*, 12.
[16] Z. Car, S. Baressi Šegota, N. Anđelić, I. Lorencin, V. Mrzljak, *Comput. Math. Methods Med.* **2020**, *2020*, 10.
[17] L. Dai, C. D. Smith, M. Foroozesh, L. Miele, Z. Qin, *Int. J. Cancer* **2018**, *142*, 2153–2162.
[18] L. Dai, J. Chen, Z. Lin, Z. Wang, S. Mu, Z. Qin, *J. Cancer.* **2020**, *11*, 4683.
[19] C. Xun, M. B. Chen, L. Qi, Z. Tie-Ning, X. Peng, L. Ning, W. Li-Wei, *J. Exp. Clin. Cancer Res.* **2015**, *34*, 1–9.

[20] K. Song, L. Dai, X. Long, X. Cui, Y. Liu, W. Di, *OncoTargets Ther.* **2019**, *12*, 4437.
[21] C. D. Britten, E. Garrett-Mayer, S. H. Chin, K. Shirai, B. Ogretmen, T. A. Bentz, M. B. Thomas, *Clin. Cancer Res.* **2017**, *23*, 4642–4650.
[22] J. Yang, C. Yang, S. Zhang, Z. Mei, M. Shi, S. Sun, C. Xie, *Cancer Biol. Ther.* **2015**, *16*, 1194–1204.
[23] S. Thakur, B. Sarkar, A. J. Ansari, A. Khandelwal, A. Arya, R. Poduri, G. Joshi, *Food Chem. Toxicol.* **2021**, *147*, 111887.
[24] G. Yang, M. Gu, W. Chen, W. Liu, Y. Xiao, H. Wang, P. Sheng, *Inflammation.* **2018**, *41*, 1498–1507.
[25] W. H. Al-Shujairi, J. N. Clarke, L. T. Davies, M. R. Pitman, J. K. Calvert, A. L. Aloia, J. M. Carr, *J. M. J. Gen. Virol.* **2019**, *100*, 629–641.
[26] R. Kurd, E. Ben-Chetrit, H. Karameh, M. Bar-Meir, **2020**, medRxiv. DOI:10.1101/2020.06.20.20099010.
[27] L. Lisi, P. M. Lacal, M. L. Barbaccia, G. Graziani, *Biochem. Pharmacol.* **2020**, 114169.
[28] L. H. Al-Wahaibi, H. M. Hassan, A. M. Abo-Kamar, H. A. Ghabbour, A. A. El-Emam, *Molecules.* **2017**, *22*, 710.
[29] H. M. Hassan, L. H. Al-Wahaibi, G. S. Shehatou, A. A. El-Emam, *Am. J. Cancer Res.* **2021**, *11*, 350–368.
[30] K. Anand, G. J. Palm, J. R. Mesters, S. G. Siddell, J. Ziebuhr, R. Hilgenfeld, *The EMBO J.* **2002**, *21*, 3213–3224.
[31] H. Yang, M. Yang, Y. Ding, Y. Liu, Z. Lou, Z. Zhou, Z. Rao, *Proc. Natl. Acad. Sci. USA.* **2003**, *100*, 13190–13195.
[32] A. K. Ghosh, M. Brindisi, D. Shahabi, M. E. Chapman, A. D. Mesecar, *ChemMedChem.* **2020**, *15*, 907–932.
[33] S. K. Wong, W. Li, M. J. Moore, H. Choe, M. Farzan, *J. Biol. Chem.* **2004**, *279*, 3197–3201.
[34] B. Hu, L. P. Zeng, X. L. Yang, X. Y. Ge, W. Zhang, B. Li, Z. L. Shi, *PLoS Pathog.* **2017**, *13*, e1006698.
[35] B. Korber, W. M. Fischer, S. Gnanakaran, H. Yoon, J. Theiler, W. Abfalterer, D. C. Montefiori, *Cell.* **2020**, *182*, 812–827.
[36] J. A. Plante, Y. Liu, J. Liu, H. Xia, B. A. Johnson, K. G. Lokugamage, P. Y. Shi, *Nat. Protoc.* **2021**, *16*, 1761–1784.
[37] L. Yurkovetskiy, X. Wang, K. E. Pascal, C. Tomkins-Tinch, T. P. Nyalile, Y. Wang, J. Luban, *Cell.* **2020**, *183*, 739–751.
[38] L. Tang, A. Schulkins, C. N. Chen, K. Deshayes, J. S. Kenney, doi: 10.20944/preprints202005.0407.v1.
[39] T. Huynh, H. Wang, B. Luan, *J. Phys. Chem. Lett.* **2020**, *11*, 4413–4420.
[40] T. Huynh, H. Wang, B. Luan, *Phys. Chem. Chem. Phys.* **2020**, *22*, 25335–25343.
[41] Ž.B. Milanović, M. R. Antonijević, A. D. Amić, E. H. Avdović, D. S. Dimić, D. A. Milenković, Z. S. Marković, *RSC Adv.* **2021**, *11*, 2838–2847.
[42] D. A. Milenković, D. S. Dimić, E. H. Avdović, Z. S. Marković, *RSC Adv.* **2020**, *10*, 35099–35108.
[43] C. A. Lipinski, F. Lombardo, B. W. Dominy, P. J. Feeney, *Adv. Drug Delivery Rev.* **1997**, *23*, 3–25.
[44] Z. Jin, X. Du, Y. Xu, Y. Deng, M. Liu, Y. Zhao, H. Yang, *Nature.* **2020**, *582*, 289–293.
[45] D. A. Milenković, D. S. Dimić, E. H. Avdović, Z. S. Marković, *RSC Adv.* **2020**, *10*, 35099–35108.
[46] X. Du, Y. Li, Y. L. Xia, S. M. Ai, J. Liang, P. Sang, S. Q. Liu, *Int. J. Mol. Sci.* **2016**, *17*, 144.
[47] A. Fischer, M. Sellner, S. Neranjan, M. Smieško, M. A. Lill, *Int. J. Mol. Sci.* **2020**, *21*, 3626.
[48] Z. Zhang, Y. Shi, H. Liu, *Biophys. J.* **2003**, *84*, 3583–3593.
[49] M. G. Pikkemaat, A. B. Linssen, H. J. Berendsen, D. B. Janssen, *Protein Eng.* **2002**, *15*, 185–192.
[50] M. Kokkinidis, N. M. Glykos, V. E. Fadouloglou, *Adv. Protein Chem. Struct. Biol.* **2012**, *87*, 181–218.
[51] N. Homeyer, H. Gohlke, *J. Comput. Chem.* **2013**, *34*, 965–973.
[52] H. L. N. de Amorim, R. A. Caceres, P. A. Netz, *Curr. Drug Targets* **2008**, *9*, 1100–1105.

Submitted: May 28, 2021
Accepted: August 18, 2021